Rashba-driven anomalous Nernst conductivity of high spin-orbit-coupled lead chalcogenide films

Parijat Sengupta and Junxia Shi
Department of Electrical and Computer Engineering, University of Illinois, Chicago, Illinois 60607, USA

(Received 12 February 2018; published 29 June 2018)

In the absence of external magnetization, a finite Berry curvature [$\Omega(k)$] in the role of a momentum-dependent magnetic field can lead to a Hall-type thermal behavior such as the anomalous Nernst effect. The traditional and nonanomalous variants require a real-space magnetic field. In this work, we report coefficients for the anomalous Nernst effect (ANE) and its spin analog, a variant of the more well-established spin Nernst effect (SNE) in lead chalcogenide (*PbX*; X = S, Se, Te) films. The narrow gapped *PbX* films with a large spin-orbit coupling (soc) offer a significant Rashba interaction that gives rise to $\Omega(k)$ and the attendant anomalous thermal behavior. In the presence of a temperature gradient, the ANE and SNE establish a thermal and spin current and are characterized by their respective coefficients which acquire higher values for a stronger Rashba interaction. We further show that an extrinsic soc generated by an in-plane electric field offers a gate-like mechanism to control (and turn-off) the anomalous thermal currents. Finally, we conclude by deriving the efficiency of an ANE-driven low-temperature Carnot heat engine and demonstrate that it can be gainfully optimized in systems with a robust intrinsic soc resulting in low carrier effective masses. Cooling techniques in microdevices via $\Omega(k)$ regulated anomalous thermal conductivity contributions are briefly discussed.

DOI: 10.1103/PhysRevMaterials.2.064606

I. INTRODUCTION

The Nernst effect (NE) describes the generation of a transverse electric field by a longitudinal temperature gradient in presence of an out-of-plane magnetic field. The related Nernst coefficient is nominally expressed as $\mathcal{N} = E_y/(-\nabla_x T)$ [1]. The Nernst-induced electric field and the temperature gradient exist along the y and x axes, respectively. A variant of NE in the absence of a real-space magnetic field has also been observed [2]; the magnetic field instead, is supplied by an analogous quantity—the Berry curvature [3]. The Berry curvature [$\Omega(k)$] as an effective magnetic field in momentum space (k) imparts a Lorentz force on carrier electrons and is the precursor to a variety of observed phenomena, an illustration of which is the anomalous Nernst effect (ANE). Succinctly, when a Hall current flows in the presence of a temperature gradient and a Berry curvature aided magnetization, the effects are collectively grouped under anomalous thermoelectric behavior. The current, in case, it is of spin-type generates the anomalous spin Nernst effect, while the more conventional charge variant manifests as the aforementioned ANE. The genesis of these anomalous Hall phenomena discernible through their unique transport signatures lies in the creation of a Berry (anomalous) velocity, $v_{\text{ane}} \propto \mathbf{E} \times \Omega(k)$, in the presence of a local electric field, $\mathbf{E}$. This "extra" and anomalous term modifies the equation of motion for an electron wave packet. As such, the ANE, in particular, has been theoretically predicted in a wide selection of materials including the d-density wave state in cuprate superconductors [4], illuminated graphene [5], and monolayer group-VI dichalcogenides [6]. For a comprehensive review of the Nernst effect within the Fermi liquid picture, see, for example, Ref. [7].

In each of the aforementioned family of materials, it is possible to write a prototypical Hamiltonian transformable along a closed contour in momentum space in a cyclic adiabatic process giving rise to the nonzero Berry connection [$\mathcal{A}(k)$] from which an equivalent magnetic field [$\Omega(k) = \nabla_k \times \mathcal{A}(k)$] can be defined. For the case of graphene-like materials and the single-layer metal dichalcogenides, in the presence of either broken inversion or time-reversal symmetry (TRS), the form of Hamiltonian that sets up a finite $\Omega(k)$ is of a massive Dirac-type [8,9]: $\mathcal{H}_{\text{eff}} = \nu(\sigma_x k_y - \sigma_y k_x) + \Delta\sigma_z$. The constant ν has units of eVÅ and Δ is the generalized Dirac mass. The Pauli matrices (σ_i) may act on the lattice or spin subspace. It is easy to note, however, that the form of the k-dependent part of the Hamiltonian that permits a finite $\Omega(k)$ also describes the linear Rashba spin-orbit coupling (RSOC) for Bloch conduction electrons [10,11]. For a set of conduction electrons in a thin film (quantum well) that follow a quadratic dispersion and split into the linear RSOC-induced spin-polarized subbands, it is therefore reasonable to anticipate the occurrence of a similarly definable $\Omega(k)$. The $\Omega(k)$ that lies at the heart of anomalous thermal effects, in this case, is solely an outcome of the linear RSOC Hamiltonian; the quadratic term does not contribute. A nonvanishing $\Omega(k)$ therefore alludes to the appearance of a concomitant ANE, the analytic estimation of which is the chief purpose here. We quantitatively estimate the strength of ANE in thin films whose Bloch conduction bands are split by RSOC in spin-polarized ensembles and examine underlying dependencies that enhance this thermomagnetic process.

An additional purported aim is also to uncover avenues that potentially optimize the efficiency of ANE via changes to strength of RSOC, the band curvature (tied to film dimensions), and external impurities. In fact, since an avowed goal in recent times hinges on the design of "energy-harvesting" techniques [12], a large ANE can complement the NE in miniaturized magnetothermal devices. It is worthwhile though to emphasize that while a definite $\Omega(k)$ is derivable from a RSOC Hamiltonian and assumes an identical form to that obtained

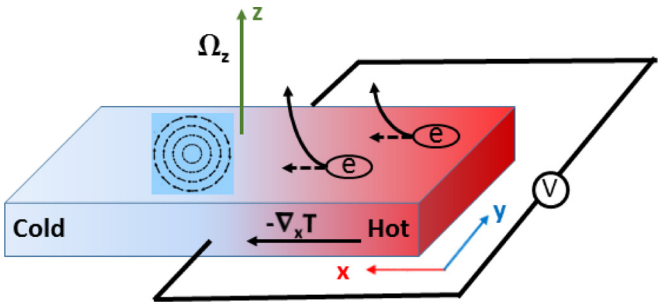

FIG. 1. A schematic depiction of the anomalous Nernst effect in a PbTe (representative *PbX*) slab with a temperature gradient along the x axis. The Rashba coupled Bloch conduction electrons with the chiral in-plane spin polarization shown on the slab surface as a concentric pattern generates $\Omega(k)$, a momentum-dependent magnetic field along the z axis (out-of-plane). An external z-axis aligned magnetic field (not shown) is also applied to the PbTe slab. An anomalous voltage develops in a direction transverse (y axis) to $\nabla_x T$. A key aspect in this setup is the manipulation of the spin-polarization via an electric field. PbTe fulfills this requirement by virtue of a large Rashba coupling coefficient.

for gapped graphene-like materials and dichalcogenides [9], the genesis of it here lies in the spin degree of freedom unlike an inversion breaking mixing of orbitals in the latter. This disparity in the origin of the emergence of $\Omega(k)$ aside, it is significant to observe that RSOC is only operational when inversion symmetry is lost, which essentially constitutes one of the prerequisites (the other is TRS and at least one must be satisfied) for a nonvanishing $\Omega(k)$ and fulfilled by the graphene family and dichalcogenides. Evidently, for a discernible $\Omega(k)$ (and ANE), a primary requirement centers around a large RSOC, a quantity generally pronounced in confined structures of compounds with narrow band gaps and high intrinsic spin-orbit coupling. While several sets of materials display a robust RSOC, it is beneficial to recall the thermal basis of the parent NE and thus select a candidate system that also combines favourable thermoelectric behavior. The lead chalcogenides [13]—*PbX* (X = S/Se/Te)—conform well in this regard, possessing the necessary material attributes for a large RSOC and a high thermoelectric figure of merit (ZT). In this family PbTe and its alloyed derivatives have been widely researched for achieving an enhanced ZT [14]. As additional corroboration of the heightened interest, PbTe Peltier cells offer the maximum efficiency [15] to date.

In an n-doped PbTe sample under an out-of-plane magnetic field (causing a Zeeman split) and a temperature gradient (Fig. 1), we show that the ANE responds to a Rashba-controlled Berry curvature distribution in momentum space and can be further modulated with an in-plane electric field. A complete cessation of ANE [vanishing $\Omega(k)$] happens when an in-plane electric field initiated spin-orbit coupling (soc) exactly annuls the Zeeman splitting. An accompanying quantifiable spin current—the phenomenon of spin Nernst effect—also flows mirroring the pattern observed for ANE. In the last part, we develop the idea of an ANE-driven Carnot engine whose efficiency is shown to be optimized by low carrier effective masses—the hallmark of high soc that also greatly influences RSOC.

We must note that both Rashba and the Zeeman splitting are essential for the production of anomalous Nernst and the class of spin Nernst effect discussed here. The linear Rashba Hamiltonian allows a Berry phase in odd-multiples of π while the Zeeman splitting furnishes a band gap necessary for the Berry curvature. A zero-gap ($\Delta = 0$) Hamiltonian as shown below [see Eq. (4)] has no Berry curvature. Further, both these splits operate independent of each other; specifically, the bands are separated horizontally along the k axis in the case of Rashba spin-orbit coupling and moved vertically when a z-directed magnetic field causes a Zeeman-split. As is well-understood, the Zeeman splitting leads to spin polarization (unequal spin-up and spin-down) while being conspicuously absent for the Rashba spin-orbit Hamiltonian. This being simply a consequence of the breaking of time reversal symmetry in the former.

II. ANOMALOUS NERNST AND SPIN NERNST EFFECT

For an analytic formulation, we begin by writing the expression for ANE which is $J_y = \mathcal{N}'(-\nabla_x T)$. The primed coefficient N' distinguishes from $\mathcal{N}$, the corresponding notation for NE. The ANE coefficient is [16]

$$\mathcal{N}' = \frac{ek_B}{\hbar} \sum_{\pm} \int \frac{d^2\mathbf{k}}{4\pi^2}\, \Omega(k)\, \mathcal{S}(k), \tag{1}$$

where $\mathcal{S}(k)$ is the entropy density. The Boltzmann constant is k_B. The entropy density is defined as: $\mathcal{S}(k) = -f_k \ln f_k - (1 - f_k)\ln(1 - f_k)$. Here, f_k is the usual Fermi distribution function. The summation over the spin-split bands is indicated by $\pm$ under the $\sum$ operator. As an insight and a heuristic reasoning into the particular form of the ANE coefficient [Eq. (1)], we simply note that a finite $\Omega(k)$ lets the electron carriers (of charge "e" and in the presence of an electric field $\mathbf{E}$) acquire an additional "anomalous" velocity $v_{\text{ane}} = (e\mathbf{E}/\hbar) \times \Omega(k)$. Multiplying v_{ane} by the entropy density furnishes the coefficient for the transverse heat current from which we obtain by a direct application of Onsager relation, the coefficient $\mathcal{N}'$ in Eq. (1). The electric field that we allude to while expressing the anomalous velocity is internally set up as a response to the diffusion current on account of the temperature gradient. The response, in an open-circuit case, being an electric field that sets up an equal and opposite drift current. Note that the Nernst effect is usually measured when there are no net current components. For an exact reproduction of Eq. (1), the interested reader can follow the steps outlined in Refs. [2,4]. The program therefore, to proceed further with ANE calculations is a determination of $\Omega(k)$. To do so, we first write down the minimal Hamiltonian that describes the Rashba and Zeeman spin-split parabolic conduction bands in a *PbX* quantum well. It is simply given by

$$H_0 = \frac{p^2}{2m^*} + \alpha_R(\sigma_x k_y - \sigma_y k_x) + \Delta\sigma_z. \tag{2}$$

The Pauli matrices in Eq. (2) act on the spin-space and the parameter Δ is the out-of-plane magnetic field governed Zeeman splitting. Note that the Zeeman splitting ($\Delta\sigma_z$) fulfills the role of the generalized Dirac mass mentioned before. The Rashba coupling parameter is α_R with adjustable strength via a gate electrode while the effective mass is m^* for the

L-valley conduction electrons of a PbX film (quantum well confined along the z axis). The corresponding eigen states are $\varepsilon_{\pm} = p^2/2m^* \pm \alpha_R k \pm \Delta$. The upper (lower) sign is for the spin-up (down) band. Additionally, the Hamiltonian H_0 only considers the conduction electrons (CE) of the PbX film (rock salt crystal structure) that belong to the L-valley and whose axis coincides with the [111] direction. Note that there exist three other oblique valleys with axes mis-aligned to the [111] vector [17]. In general, the three oblique L-valleys are marked by an effective mass different from carriers resident in the longitudinal valley. The calculations that follow use material parameters describing the longitudinal valley. We make use of a 4×4 $k.p$ Hamiltonian [18,19] that captures the dispersion around the high-symmetry L-valley; substituting for the confined $k_z = -i\partial_z$ in the Hamiltonian and followed by a numerical diagonalization supplies the quantum well CE effective mass [17]. The presented calculations use PbTe as the representative PbX.

For a quantum well, which is a two-dimensional system whose Hamiltonian [disregarding the quadratic component that does not contribute to $\Omega(k)$] is expressible as $H(k) = \mathbf{d}(\mathbf{k}) \cdot \sigma$, the Berry curvature is defined by the relation [20]

$$\Omega_{\mu\nu} = \tfrac{1}{2}\varepsilon_{\alpha\beta\gamma}\hat{d}_\alpha(\mathbf{k})\partial_{k_\mu}\hat{d}_\beta(\mathbf{k})\partial_{k_\nu}\hat{d}_\gamma(\mathbf{k}), \tag{3}$$

where $\hat{\mathbf{d}}(\mathbf{k}) = \frac{\mathbf{d}(\mathbf{k})}{d(k)}$. Applying this formalism in the case of Rashba Hamiltonian [Eq. (2)], and noting that the vector $\mathbf{d}$ in component form is $(\alpha_R k_y, -\alpha_R k_x, \Delta)$, a direct substitution in Eq. (3) lets us write $\Omega(k)$ as

$$\Omega(k) = \pm\frac{\alpha_R^2 \Delta}{2[(\alpha_R k)^2 + \Delta^2]^{3/2}}\hat{\mathbf{z}}. \tag{4}$$

In Eq. (4), $k^2 = k_x^2 + k_y^2$. The upper (lower) sign is for the spin-down (up) band. The Ω as a momentum-dependent magnetic field points out-of-plane (the z axis). The $\Omega(k)$ vanishes as $\Delta \to 0$; the quenching of Δ (the Zeeman splitting) in this case restores TRS from which follows the relation, $\Omega(k) = 0$. A simple inspection of Eqs. (1) and (4) reveals that for a significant ANE a large $\Omega(k)$ is desirable which in turn requires a sizable Rashba splitting determined via the strength of the coefficient, α_R. The Rashba coefficient is strong in narrow band gap materials with considerable intrinsic soc, such as those belonging to the PbX family. The Rashba coupling coefficient is expressed as : $\alpha_R = \lambda_0\langle F(z)\rangle$, where $\langle F(z)\rangle$ is the average out-of-plane (z axis) electric field. The average value for $\langle F(z)\rangle$ is $\frac{en}{\epsilon\epsilon_0}$. Here, e is the electronic charge, the dopant density is n, and ϵ identifies the dielectric constant. The permitivity of free space is ϵ_0. The material-dependent λ_0 is given as [21]

$$\lambda_0 = \frac{\hbar^2}{2m^*}\frac{\Delta_{\rm so}}{E_g}\frac{2E_g + \Delta_{\rm so}}{(E_g + \Delta_{\rm so})(3E_g + 2\Delta_{\rm so})}. \tag{5}$$

For the specific case of PbX quantum wells, the parameters in Eq. (5) are defined for the longitudinal L-valley; here, E_g is the direct band gap, the intrinsic soc is $\Delta_{\rm so}$, and m^* denotes the conduction band effective mass. The tuning of α_R is therefore, unlike, the intrinsic soc possible via changes to the band gap and effective mass in confined structures.

Before we carry out a quantitative analysis of the anomalous thermal behavior, a set of remarks are in order: First (1), the dielectric constant (dc) of PbTe is abnormally large ($\approx$400), an outcome attributed to the high-polarizability of the chemical bond. This high dc [22] in addition to determining α_R via $\langle F(z)\rangle$ also couples with the low effective electron masses (in part, attributed to a substantial intrinsic soc) to set up a significant Bohr radius [23] and thus enhancing carrier mobility. While thermoelectric applications require a pronounced mobility (and low thermal conductivity) for an optimized thermoelectric figure-of-merit (ZT), for the Rashba-driven ANE, a change in dc is also reflected in α_R which clearly revises $\Omega(k)$ and consequently the thermal anomalous effects. The dc has been shown [24] to be adjustable via simple lattice deformations of the rock salt crystal. In passing, it is useful to mention that polarizable PbX bonds also typically scupper the thermal conductivity to improve ZT. The second comment (2) pertains to additional soc terms that may occur in the Hamiltonian [Eq. (2)]. An extra soc-term (besides Rashba) for an in-plane electric field ($F_{\rm ip}$) can be of the form $e\beta\hat{\sigma} \cdot (\mathbf{F}_{\rm ip} \times \mathbf{k})$. The complete Hamiltonian is then of the type

$$H_0 = \frac{p^2}{2m^*} + \alpha_R(\sigma_x k_y - \sigma_y k_x) + \Delta\sigma_z + e\beta\hat{\sigma} \cdot (\mathbf{F}_{\rm ip} \times \mathbf{k}). \tag{6}$$

Here, β is the constant for an electric field induced spin-orbit coupling. For an x-axis directed $F_{\rm ip}$, the last term in Eq. (6) contributes to the overall Hamiltonian by augmenting the Dirac mass/band gap (Δ); it then changes to $\Delta + e\beta F_{\rm ip}k_y\sigma_z$. The corresponding expression for $\Omega(k)$ by a direct application of the formula in Eq. (3) gives

$$\Omega(k) = \pm\frac{\alpha_R^2(\Delta + e\beta F_{\rm ip}k_y)}{2[(\alpha_R k)^2 + (\Delta + e\beta F_{\rm ip}k_y)^2]^{3/2}}\hat{\mathbf{z}}. \tag{7}$$

Note that in the above equation, we simply replaced the band gap in Eq. (4) by its amended value given above.

A more appealing situation emerges for an in-plane electric field solely directed along the y-axis; the soc in this case is simply $-e\beta F_{\rm ip}k_x\sigma_z$ and manifestly counteracts Δ, the Zeeman splitting. For values of the y directed $F_{\rm ip}$ such that $\Delta - e\beta F_{\rm ip}k_x \to 0$, the out-of-plane ($z$ axis) magnetic field induced broken TRS is restored. The fulfillment of TRS, which we pointed out before, leads to a complete ceasing of $\Omega(k)$ (under inversion symmetry) and the attendant ANE. It is also apparent [from Eq. (7)] that a union of the spin-orbit Hamiltonians through their respective coupling coefficients, α_R and β, allows a more detailed measure of control over the ANE-governed charge current (in a closed circuit). In fact, $\mathcal{F}_{\rm ip}$ can be considered applied from a set of in-plane ohmic contacts and serve as a threshold bias; for the correct polarity and magnitude, as $\Omega(k) \to 0$, it describes a complete turnoff setting unique to the material system. The final remark (3) considers the overall contribution of the two spin-split bands. Noting that $\Omega_\downarrow(k) = -\Omega_\uparrow(k)$, the complete ANE coefficient becomes $\mathcal{N}'_{ov} = ek_B/(4\pi^2\hbar)\int \mathbf{d}^2k\Omega_\downarrow(k)[\mathcal{S}_\downarrow(k) - \mathcal{S}_\uparrow(k)]$. It is therefore straightforward to see that a spin-up band placed energetically above its spin-down counterpart when empty (or zero entropy) maximizes the ANE.

In close conjunction to ANE and grounded on the same principle of Berry curvature fashioned thermal effects, a spin Nernst coefficient (Fig. 2) following Ref. [6] can be defined as

$$\mathcal{N}'_s = \frac{k_B}{2}\int \frac{\mathbf{d}^2k}{4\pi^2}[\Omega_\uparrow(k)\mathcal{S}_\uparrow(k) - \Omega_\downarrow(k)\mathcal{S}_\downarrow(k)]. \tag{8}$$

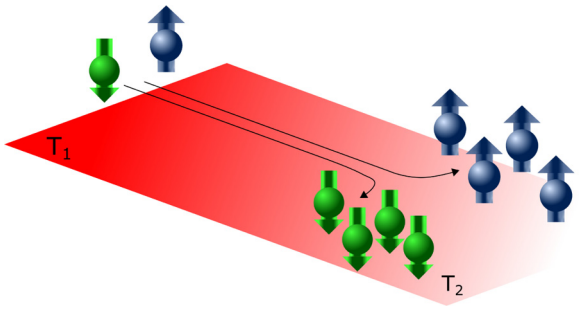

FIG. 2. The schematic shows spins (indicated by up- and down-arrows) of the conduction electrons split by the extrinsic Rashba coupling moving in opposite directions in a PbTe quantum well. The anomalous velocity component (v_{ane}) created by the Berry curvature guides the spins as shown giving rise to a finite spin current and the attendant spin Nernst effect in presence of a temperature gradient. Here, the quantum well is fitted with contacts at two different temperatures (T_1, T_2) as shown in the schematic and $T_1 > T_2$ sets up the thermal field. The momentum-dependent Berry curvature through its "magnetic-field" action serves as a bridge to interlink the external Rashba coupling to phenomena driven by temperature gradients. This coupling, in principle, establishes the elements of spin caloritronics.

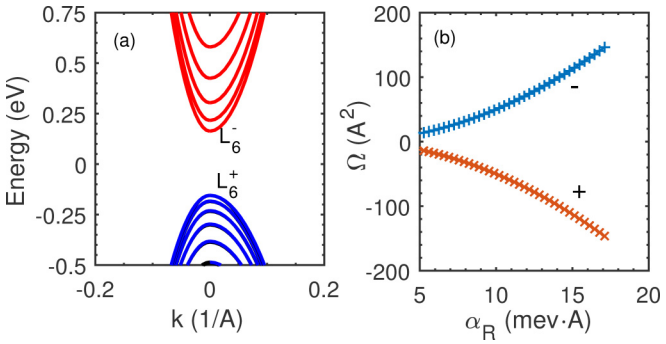

FIG. 3. The numerically obtained L-valley dispersion of a 6.0-nm wide [111] PbTe film along the high-symmetry path $\overline{K} - \overline{L} - \overline{\Gamma}$ is shown on the left panel (a). The right figure (b) plots [using Eq. (4)] the Rashba-aided Berry curvature at the conduction band minimum ($|k| = 0$) where the upper (lower) branch is for the spin-down (up) conduction state. The asymmetry-inducing electric field (out-of-plane) necessary for the Rashba splitting arises from an n-doping concentration; for purpose of numerical calculation, n was varied between $1 \times 10^{12}\,\mathrm{cm}^{-2}$ and $4 \times 10^{12}\,\mathrm{cm}^{-2}$. The dielectric constant of PbTe was set to 400 (see note below about this unusually large value). The Zeeman splitting is treated as an external parameter and set to $\Delta = 2.0\,\mathrm{meV}$ throughout.

Before expounding on the behavior of the spin Nernst effect(SNE) via its corresponding coefficient in Eq. (8), recall that this refers to the flow of a transverse spin current due to an applied temperature gradient—an exact parallel of the spin Hall effect produced by an external field. The SNE, first observed in thermopower measurements in platinum films (a nonmagnetic material suffices) does not require an external magnetic field. It is beneficial to reiterate that the $\Omega(k)$ in Ref. [6] strictly arises from the broken inversion symmetry of the monolayer transition metal dichalcogenide (TMDC), unlike the Rashba-governed case which relies on an electric field (supplied externally or through the truncation of the bulk crystal potential in a nanostructure) to introduce asymmetry. In both systems, however, it leads to the flow of a temperature gradient powered spin current via oppositely-polarized spins which live in vicinity of the K and K' edge in a TMDC monolayer and those which are Rashba-split around the bottom of the PbX L-valley conduction band.

III. RESULTS

For a numerical estimate of α_R, from which follows the $\Omega(k)$ and coefficients for ANE and SNE, a 6.0-nm wide PbTe film grown along the [111] axis is selected as the model structure. The L-valley band gap and effective mass (transverse) of this film from a $k.p$ calculation are $0.0565m_0$ and 0.33 eV. The free electron mass is $m_0 = 9.1 \times 10^{-31}\,kg$. The dispersion of the 6.0-nm wide PbTe film and the accompanying Rashba-induced $\Omega(k)$ is shown in Fig. 3. Note that $\Omega(k)$ is plotted as a function of α_R, which is a function of material parameters and the film's Bloch conduction electrons effective mass.

To proceed further a number of other parameters useful in determination of $\mathcal{N}'$ and $\mathcal{N}_s'$ must be defined: We begin by assigning the temperature (T) a pair of values: $T = \{125, 300\}K$. The Fermi level is set to $E_f = 0.15\,\mathrm{eV}$ from the bottom of the conduction band while the charge/dopant density is assumed to lie between $10^{12}\,\mathrm{cm}^{-2}$ and $8 \times 10^{12}\,\mathrm{cm}^{-2}$. This dopant density furnished electric field lets α_R acquire values from 5.0 meVÅ–30.0 meVÅ. Note that for a more accurate calculation of the doping-governed electric field, a Poisson equation must be simultaneously solved with the electronic Hamiltonian; however, for just the purpose of determination of the Rashba coefficient, we resort to a simpler estimation using the Gauss law of electrostatics. Inserting these numbers in Eqs. (1) and (8), we perform a numerical integration in momentum space such that $|k| \leqslant 0.03\,\mathrm{nm}^{-1}$; the rationale behind selecting this range lies in the simple fact that entropy for higher momentum values (or equivalently energy) progressively approaches zero. For a feel of the coefficients, say at room temperature ($T = 300\,K$), using the 6.0 nm PbTe quantum well as a test vehicle, we can estimate for a preset Rashba coupling strength, set, for example, to $\alpha_R = 20.0\,\mathrm{meV} \cdot$ Å: The ANE coefficient ($\mathcal{N}'$) is then $0.0235 * ek_B/h$ while the spin Nernst coefficient ($\mathcal{N}_s'$) evaluates to $0.0470 * k_B/4\pi$. For coefficient behavior over a broad range of α_R values, we plot $\mathcal{N}'$ and $\mathcal{N}_s'$ in Fig. 4, again in units of ek_B/h and $k_B/4\pi$, respectively. We only show the ANE coefficient for the spin-down band since the contribution of the spin-up band differs marginally from the former and carries a reversed sign. The closeness is simply an outcome of the moderate energy difference between the spin-split bands. Separately, the plot clearly reveals a more substantial display of ANE and SNE for a weightier α_R, which expressly influences and enlarges $\Omega(k)$ - the engine behind anomalous effects. We make a note here that the parameter α_R, in addition to dopant density changes is also amenable to further modification via adjustments to m^*, the band gap (E_g), and the intrinsic soc. While the soc is admittedly harder to modulate, however, m^* and E_g through varying degrees of confinement, layered-heterostructure design, and strain-like perturbation can substantially augment α_R. In line with

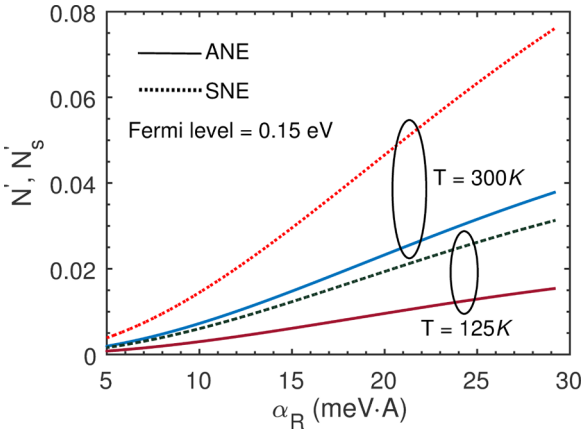

FIG. 4. The ANE ($\mathcal{N}^{'}$) and SNE ($\mathcal{N}^{'}_{s}$) coefficients are plotted in units of ek_B/h and $k_B/4\pi$, respectively. The $\mathcal{N}^{'}$ is shown only for the spin-down band. Both coefficients increase as higher values of α_R are realized through doping or an external gate electrode. Additionally, at elevated temperatures that raise the entropy, larger coefficients are obtained. While the overall $\mathcal{N}^{'}$ taking both spin split bands into account nearly vanishes, the SNE allows the flow of a net spin current.

schemes that may reinforce the anomalous thermal behavior, it is also expedient to identify regions in momentum-space where $\Omega(k)$ and $\mathcal{S}(k)$ attain their highest values. The $\Omega(k)$ from Eq. (4) has a Lorentzian spread centered around the $|k| = 0$ point, which is the conduction band origin and reaches its maximum; likewise, the entropy has peaks on the Fermi surface and tails off away from it. For these two variables to amplify ANE and SNE, an intersecting region of momentum space must therefore be chosen to locate carriers with energy closely aligned to the Fermi surface while simultaneously ensuring that it isn't too far away from $|k| = 0$ for a reasonable $\Omega(k)$.

As a more definitive guide that ascertains the efficiency (η = output/input) of ANE, we can construct a paradigmatic Carnot engine like abstraction into which heat is pumped and 'useful' work extracted as power in a closed circuit. The power ("output") is $(\mathcal{N}^{'}(-\nabla_x T)^2\mathcal{R}$. The electric resistance of the closed circuit is $\mathcal{R}$. We consider a low temperature regime to ignore any phonon-driven thermal currents. A Carnot engine modeled on the NE must proceed by establishing a temperature gradient, where the desired heat current ("input") to maintain a temperature difference is given by the standard Fourier law : $J_Q = -\kappa_{xx}\nabla_x T$. Here, κ_{xx} is the longitudinal thermal conductivity which is connected via the Wiedemann-Franz law (WFL) to its electric counterpart [25]. Briefly, the electric conductivity (for energy ε) using the linearized Boltzmann equation is [26]

$$\sigma = \frac{e^2 v_f^2}{2}\int d\varepsilon D(\varepsilon)\tau(\varepsilon)\left(-\frac{\partial f}{\partial \varepsilon}\right) = \frac{e^2 v_f^2 D(\varepsilon_f)\tau(\varepsilon_f)}{2}. \quad (9)$$

In writing the condensed expression for conductivity at Fermi energy (ε_f) [the second step of Eq. (9)], we tacitly assume that for low temperatures the parenthetically enclosed partial derivative can be approximated as $\delta(\varepsilon - \varepsilon_f)$, thus eliminating the integral in the preceding step. The density-of-states, $D(\varepsilon)$, ignoring the linear Rashba and Zeeman term is $m^*/(\pi\hbar^2)$ and the Fermi velocity (v_f) is $\hbar k/m^*$. The scattering time is $\tau(\varepsilon)$. A direct application of WFL therefore gives the longitudinal thermal conductivity as $\kappa_{xx} = \mathcal{L}\sigma T$, where $\mathcal{L} = 2.44 \times 10^{-8}\, W\Omega K^{-2}$ is the Lorentz number. By following the outlined sequence of steps, the quantity η for the proposed Carnot engine is

$$\eta_{\text{Carnot}} = \frac{2\pi\hbar^2[N^{'2}\nabla_x T]\mathcal{R}}{\mathcal{L}e^2 v_f^2 m^* \tau T}. \quad (10)$$

It is clearly noticeable from Eq. (10) that a low-effective mass improves efficiency—a result that ties well with the requirement of a strong Rashba coupled material, as both arise in compounds with a large intrinsic soc. A caveat about the Lorenz number must be included here: We quoted a value for $\mathcal{L}$ generally assumed to be true for degenerate metals and semiconductors; however, significant deviations have been recorded in a variety of set ups warranting a careful selection of the aforesaid constant in context of the system under study. For a recent work that examines such deviations, see, Ref. [27].

The aforementioned Carnot engine presented as an abstraction is marked by a certain measure of efficiency (η). Heat is pumped in and a finite (anomalous) current flow describes the overall energy cycle and the linked η parameter. We can also devise a similar abstraction and ask for the efficiency of a cycle that considers exclusively heat processes and their distribution within the system. To see this, recall that in addition to $\mathcal{N}^{'}$, the $\Omega(k)$ also introduces a transverse (to the longitudinal temperature gradient) flow of heat current now recognized as the anomalous thermal Hall effect. The corresponding anomalous thermal Hall conductivity coefficient is written as [28]

$$\kappa_{xy} = \frac{k_B^2 T}{\hbar}\int \frac{\mathbf{d}^2 k}{4\pi^2}\Omega(k)\Big[\frac{\pi^2}{3} + f\ln^2(1/f - 1) - \ln^2(1-f) - 2\text{Li}_2(1-f)\Big]. \quad (11)$$

In Eq. (11), $\text{Li}_n(x) = \sum_{m=1}^{\infty}\frac{x^m}{m^n}$ is the polylogarithmic function. As before, f denotes the equilibrium Fermi distribution. Qualitatively, the efficiency ($\eta^{'}$) for this Carnot engine, analogous to Eq. (10), is evidently a function of $\phi(\kappa_{xy},\kappa_{xx})$ as a measure of the transverse heat current for every unit of the "pumped" longitudinal component (via $\nabla_x T$). The usefulness of such efficiency calculations as a predictive guide from an application standpoint stems not only, bearing in mind the possibility of improved on-chip cooling in microelectronic structures through greater heat dissipation, but the accompanying prospects of a magnetically-controlled heat flow—the magnet here again being the topology-governed $\Omega(k)$.

IV. CONCLUDING REMARKS

To summarize, we obtain analytic expressions for anomalous Nernst and spin Nernst coefficients tunable via a nontrivial dependence on the extrinsic Rashba spin-orbit coupling created Berry curvature in PbTe films. The ease of measurement and detection of the anomalous Nernst phenomena and is spin-variant is contingent on the magnitude of their respective coefficients, which follows the distribution of $\Omega(k)$ in the

Brillouin zone. The coefficients are therefore expected to be strongest at points where $\Omega(k)$ peaks, which is the crossing of the Rashba-split bands at the conduction band minimum. Similarly, it is reasonable to assume that narrow-gap and strongly spin-orbit coupled III-V materials such as InAs or InSb can give rise to comparable anomalous thermal currents. Besides, the SNE-origin anomalous spin current may find applications in spin caloritronics [29,30] for a more diverse set of PbTe-like materials, rather than being limited, as it is hitherto, to mostly magnetic systems [31]. Moreover, a large efficiency is expected of processes that rework thermoelectric energy to manifest as dissipation-less spin currents [32]—through phenomena such as SNE—deemed useful in several applications including modern memory architectures and data storage schemes.

The SNE coefficient is also indicative of the fact that methods and materials which boost its magnitude can be desirable components of thermoelectric and spin-caloritronic device designs. The presented results when appropriately enhanced through material design may also expand the work [33,34] done with another class of compounds, the noncollinear antiferromagnets Mn_3X (X = Sn, Ge, Ga), which similarly promise a large anomalous Nernst and spin Nernst effect. In this context we may observe that while $\Omega(k)$ and consequently the anomalous coefficients diminish with decreasing intrinsic spin-orbit coupling, simply mirroring the reliance of the Rashba coupling on the former. An important implication of this dependence can, however, manifest as altered spin-relaxation times (detailed analytic calculations are deferred for a future work) for the thermally generated spin currents.

Lastly, we make an important qualitative observation in light of the presented work: The carriers in the chosen *PbX* class of compounds acquire a $\Omega(k)$ via external soc and is distinct in its origin *vis-à-vis* of the kind that exists in a gapped graphene-like material. However, exfoliated monolayers of transition metal dichalcogenides (compounds such as WS_2 that we made a note of above) which are marked by significant intrinsic soc may exhibit a discernible RSOC triggering a $\Omega(k)$ identical to the one analyzed for the *PbX* family. This additional $\Omega(k)$ may act in tandem with its counterpart generated through loss of inversion symmetry to augment the ANE and SNE coefficients. Notice that the low soc of graphene precludes the observation of a spin-promoted $\Omega(k)$ unlike, say, for example, in the TMDC, WS_2. A quantitative analysis may reveal further intricacies and general guidelines desirable for a synergy-pairing of the two Berry curvatures and their joint control through coupling to optical and magnetic fields.

[1] A. Abrikosov, *Fundamentals of the Theory of Metals* (Courier Dover, Mineola, NY, 2017).
[2] D. Xiao, Y. Yao, Z. Fang, and Q. Niu, Phys. Rev. Lett. **97**, 026603 (2006).
[3] M. Gradhand, D. Fedorov, F. Pientka, P. Zahn, I. Mertig, and B. Györffy, J. Phys.: Condens. Matter **24**, 213202 (2012).
[4] C. Zhang, S. Tewari, V. M. Yakovenko, and S. Das Sarma, Phys. Rev. B **78**, 174508 (2008).
[5] X. Zhou, Y. Xu, and G. Jin, Phys. Rev. B **92**, 235436 (2015).
[6] X.-Q. Yu, Z.-G. Zhu, G. Su, and A.-P. Jauho, Phys. Rev. Lett. **115**, 246601 (2015).
[7] K. Behnia, J. Phys.: Condens. Matter **21**, 113101 (2009).
[8] M. Ezawa, Phys. Rev. Lett. **109**, 055502 (2012).
[9] D. Xiao, G.-B. Liu, W. Feng, X. Xu, and W. Yao, Phys. Rev. Lett. **108**, 196802 (2012).
[10] N. Averkiev, L. Golub, and M. Willander, J. Phys.: Condens. Matter **14**, R271 (2002).
[11] R. Winkler, *Spin-Orbit Coupling in Two-Dimensional Electron and Hole Systems* (Springer, New York, 2003).
[12] A. B. Cahaya, O. A. Tretiakov, and G. Bauer, IEEE Trans. Magn. **51**, 1 (2015).
[13] I. I. Ravich, *Semiconducting Lead Chalcogenides*, Vol. 5 (Springer Science & Business Media, New York, 2013).
[14] Z. Dughaish, Physica B: Condensed Matter **322**, 205 (2002).
[15] K. Biswas, J. He, I. D. Blum, C.-I. Wu, T. P. Hogan, D. N. Seidman, V. P. Dravid, and M. G. Kanatzidis, Nature **489**, 414 (2012).
[16] Y. Xu, X. Zhou, and G. Jin, Appl. Phys. Lett. **108**, 203104 (2016).
[17] See Supplemental Material at http://link.aps.org/supplemental/10.1103/PhysRevMaterials.2.064606 for [brief description].
[18] J. Dimmock and G. Wright, Phys. Rev. **135**, A821 (1964).
[19] I. Kang and F. W. Wise, JOSA B **14**, 1632 (1997).
[20] S.-Q. Shen, *Topological Insulators*, Vol. 174 (Springer, New York, 2012).
[21] E. A. de Andrada e Silva, G. C. La Rocca, and F. Bassani, Phys. Rev. B **55**, 16293 (1997).
[22] Y. Kanai and K. Shohno, Jpn. J. Appl. Phys. **2**, 6 (1963).
[23] J. Heremans, R. Cava, and N. Samarth, Nat. Rev. Mater. **2**, 17049 (2017).
[24] H. W. Leite Alves, A. R. R. Neto, L. M. R. Scolfaro, T. H. Myers, and P. D. Borges, Phys. Rev. B **87**, 115204 (2013).
[25] P. Sengupta, Y. Tan, G. Klimeck, and J. Shi, J. Phys.: Condens. Matter **29**, 405701 (2017).
[26] B. R. Nag, *Electron Rransport in Compound Semiconductors*, Vol. 11 (Springer Science & Business Media, New York, 2012).
[27] M. Thesberg, H. Kosina, and N. Neophytou, Phys. Rev. B **95**, 125206 (2017).
[28] D. L. Bergman and V. Oganesyan, Phys. Rev. Lett. **104**, 066601 (2010).
[29] G. Bauer, E. Saitoh, and B. J. Van Wees, Nat. Mater. **11**, 391 (2012).
[30] S. R. Boona, R. C. Myers, and J. P. Heremans, Energy Environ. Sci **7**, 885 (2014).
[31] M. Weiler *et al.*, Phys. Rev. Lett. **108**, 106602 (2012).
[32] S. Murakami, N. Nagaosa, and S.-C. Zhang, Science **301**, 1348 (2003).
[33] L. Šmejkal and T. Jungwirth, arXiv:1804.05628.
[34] Y. Zhang, Y. Sun, H. Yang, J. Železný, S. P. P. Parkin, C. Felser, and B. Yan, Phys. Rev. B **95**, 075128 (2017).